

Ultrastable low-noise current amplifier: A novel device for measuring small electric currents with high accuracy

D. Drung,¹ C. Krause,¹ U. Becker,² H. Scherer,² and F. J. Ahlers²

¹Physikalisch-Technische Bundesanstalt (PTB), Abbestraße 2-12, 10587 Berlin, Germany

²Physikalisch-Technische Bundesanstalt (PTB), Bundesallee 100, 38116 Braunschweig, Germany

(Received 24 December 2014; accepted 19 January 2015; published online 11 February 2015)

An ultrastable low-noise current amplifier (ULCA) is presented. The ULCA is a non-cryogenic instrument based on specially designed operational amplifiers and resistor networks. It involves two stages, the first providing a 1000-fold current gain and the second performing a current-to-voltage conversion via an internal 1 M Ω reference resistor or, optionally, an external standard resistor. The ULCA's transfer coefficient is highly stable versus time, temperature, and current amplitude within the full dynamic range of ± 5 nA. The low noise level of 2.4 fA/ $\sqrt{\text{Hz}}$ helps to keep averaging times short at small input currents. A cryogenic current comparator is used to calibrate both input current gain and output transresistance, providing traceability to the quantum Hall effect. Within one week after calibration, the uncertainty contribution from short-term fluctuations and drift of the transresistance is about 0.1 parts per million (ppm). The long-term drift is typically 5 ppm/yr. A high-accuracy variant is available that shows improved stability of the input gain at the expense of a higher noise level of 7.5 fA/ $\sqrt{\text{Hz}}$. The ULCA also allows the traceable generation of small electric currents or the calibration of high-ohmic resistors. © 2015 AIP Publishing LLC. [<http://dx.doi.org/10.1063/1.4907358>]

I. INTRODUCTION

The accurate measurement of small direct currents is of increasing interest both for fundamental metrology and for practical applications, e.g., in dosimetry and semiconductor industry. With state-of-the-art picoammeters (picoameters), direct currents of 100 pA can be measured with an uncertainty of about 10 parts per million (ppm) at best.¹ The traceable generation of 100 pA with about 10 ppm uncertainty is typically accomplished at National Metrology Institutes (NMIs) with the capacitor charging method, a well-established primary standard technique.² The recent efforts for the redefinition of the SI unit ampere on the basis of quantum effects have led to single-electron transport (SET) devices generating currents of the order of 100 pA with uncertainties of about 1 ppm or better.^{3,4} Therefore, for the characterization of these devices, picoammeters are required that enable substantially lower uncertainties than currently achievable, preferably about 0.1 ppm at 100 pA.⁵ This is two orders of magnitude beyond the capabilities of state-of-the-art picoammeters, and still considerably better than for a measurement system assembled from laboratory standards.³

It was suggested to apply a cryogenic current comparator (CCC) with a large number of turns ($>10\,000$) for the accurate amplification of the small output current of a SET device.^{6,7} In a CCC, a superconducting quantum interference device (SQUID) serves as a low-noise null detector. At high currents, the CCC provides ultimate accuracy; uncertainties down to about 0.01 ppm are routinely achieved in CCC-based resistance calibrations. However, at sub-nA currents, noise rectification in the nonlinear SQUID may cause unacceptable systematic uncertainties, e.g., about 1 ppm at 100 pA with PTB's 14-bit CCC.^{8,9} Due to the long averaging times required, these nonlinear effects are hard to quantify.

Furthermore, they are found to be not sufficiently stable in time to be corrected for after careful system characterization.⁹ Therefore, they impose a severe, possibly insurmountable obstacle in the approach of operating a CCC with a high number of turns as an accurate amplifier for sub-nA currents.

To overcome the limitations caused by noise rectification in the SQUID, the ultrastable low-noise current amplifier (ULCA) was developed at PTB.^{10,11} The main idea is to adopt the best of different technologies. A state-of-the-art semiconductor amplifier is combined with a specially designed network of about 3000 thin-film chip resistors to obtain a user-friendly current amplifier with a very low noise level. The CCC with its absolute accuracy is used to calibrate the amplifier. Thanks to the high linearity of the amplifier's transfer coefficient, calibration can be done at high current levels where the effect of noise rectification in the SQUID is negligible. Provided that its transfer coefficient is sufficiently stable, the new device will combine CCC-like accuracy with all benefits of the semiconductor device. Furthermore, besides current amplification, the instrument can also be configured for current sourcing or for the calibration of high-ohmic resistors. The concept of this novel device is described in Sec. II and its basic configurations in Sec. III. The experimental performance is presented in Sec. IV. The issue of calibration is treated in Sec. V, and conclusions are given in Sec. VI.

II. THE ULCA CONCEPT

The basic ULCA circuit is schematically illustrated in Figure 1. The amplifier consists of two stages, the first providing a 1000-fold amplification of the current I_{IN} from a device under test (DUT) and the second performing a current-to-voltage conversion. The operational amplifiers OA1 and

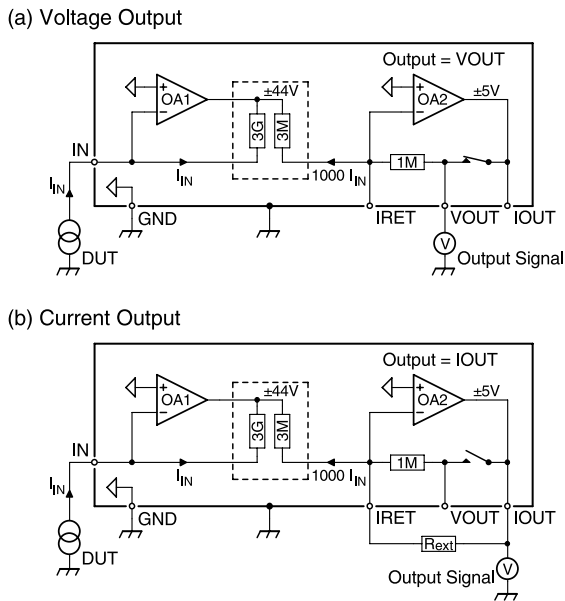


FIG. 1. Basic schematics of the ULCA. (a) Voltage output, (b) current output. The input current I_{IN} is amplified 1000 times by operational amplifier OA1 and a 3 G Ω /3 M Ω resistor network. The output stage OA2 converts the amplified current into a voltage via the internal 1 M Ω reference resistor (output = VOUT) or an external standard resistor R_{ext} (output = IOUT), respectively. The output voltage range is ± 44 V for OA1 and ± 5 V for OA2. The internal reference potential (open triangles) is connected to the ULCA's metal housing via a short on the GND connector.

OA2 in Figure 1 are sophisticated circuits comprising several monolithic op amps. This results in a low input noise level and a very high overall open-loop gain of well above 10^9 . The ± 44 V output stage of the first amplifier OA1 is realized by using discrete transistors; the required ± 47 V supply is generated from the ± 5.5 V main supply voltage via a low-power charge pump. To minimize power line interference, the ± 5.5 V supply is energized from a single 12 V lead battery housed in a remote battery box. The battery box contains two separate batteries, one of which is charged while the other is used for powering the amplifier. This enables uninterruptible battery operation and allows continuous measurements over arbitrarily long time intervals.

The total supply current drawn from the battery is 11 mA. This results in low power consumption and keeps the internal temperature close to ambient temperature. The ULCA has single-channel or dual-channel variants. Both channels in a dual-channel ULCA are completely independent from each other, including separate batteries and temperature sensors. Besides minimizing power on the ULCA printed-circuit board (PCB), special care was taken to keep the power as constant as possible, i.e., independent of the output signal, to avoid nonlinearities from thermal interaction between output and input stages of the amplifiers OA1 and OA2. This ensures that the high overall gains calculated from the individual gains of the amplifier stages are indeed achieved in practice. Consequently, the transfer coefficient of the ULCA should be constant over the full dynamic range with negligible influence from the op amps.

In normal operation, the ULCA effectively acts as a current-to-voltage converter. Its overall transresistance is

$A_{TR} = G_I R_{IV}$ where $G_I = 1000$ is the current gain of the input stage and R_{IV} is the current-to-voltage coefficient of the output stage. The latter is practically equal to the feedback resistance of the output stage, thanks to the high open-loop gain of OA2. In voltage output mode (output = VOUT), the internal 1 M Ω resistor is used for feedback, yielding $A_{TR} = 1$ G Ω . In current output mode (output = IOUT), an external standard resistor R_{ext} is applied. With the actual amplifier design R_{ext} can be chosen between a short (for example, a CCC winding during calibration) and 100 M Ω . This way, the transresistance can be increased up to 100 G Ω , or the performance can be improved if the quality of the external standard resistor exceeds that of the internal 1 M Ω metal-foil resistor.

At low values of R_{ext} , the cable resistance between the ULCA and the external standard resistor has to be considered. Four-terminal measurement can be realized by connecting the current-carrying wires of the standard resistor to OA2 (IOUT and IRET) and the voltage-sensing wires to the voltmeter. However, in this configuration, the voltmeter is connected in parallel to R_{ext} and its input resistance changes the overall transresistance accordingly. This can be practically avoided if the low-potential side of the voltmeter is connected to ground as shown in Figure 1(b), but another voltmeter is used to measure the small voltage difference between the low-potential side of the standard resistor and ground. It can be shown that the input resistance of the voltmeter at the output of OA2 has no effect due to the circuit design, and that the input resistance of the voltmeter at the standard resistor's low-potential side is strongly suppressed because of the low voltage across the voltmeter input. The requirements on the accuracy of this voltmeter are considerably relaxed compared to the instrument at the amplifier output that directly affects the measurement uncertainty.

A key component in the ULCA concept is the 3 G Ω /3 M Ω resistor network at the output of OA1. In the following, it will be simply referred to as "3 G Ω network" because the input resistor networks of all ULCAs implemented so far provide a 1000-fold current gain. For highest accuracy, the network is realized with NiCr thin-film resistor technology; thick-film resistors have inadequate stability and exhibit a too high voltage dependence of resistance. In the original approach,¹⁰ a large number of integrated 10 M Ω /10 k Ω matched resistor pairs in SO-8 package were considered (SO series from Powertron/Vishay Precision Group). The individual resistor pairs are fabricated on a common substrate and, consequently, are highly matched and thermally well coupled. In spite of a careful chip layout, tiny systematic differences between the high-ohmic and low-ohmic sides remained. This resulted in a non-vanishing, slightly positive temperature coefficient of G_I (about +1.3 ppm/K for the latest generation). It is not yet known whether the systematic differences also affect the long-term stability of G_I .

To minimize systematic differences between both sides of the network, an alternative approach was developed. The network is now implemented by about 3000 identical 2 M Ω thin-film chip resistors (0805 size = 2 mm \times 1.25 mm). All resistors of the network are taken from the same fabrication lot to maximize matching. The base element consists of 31 resistors in series at the high-ohmic side and 32 resistors in

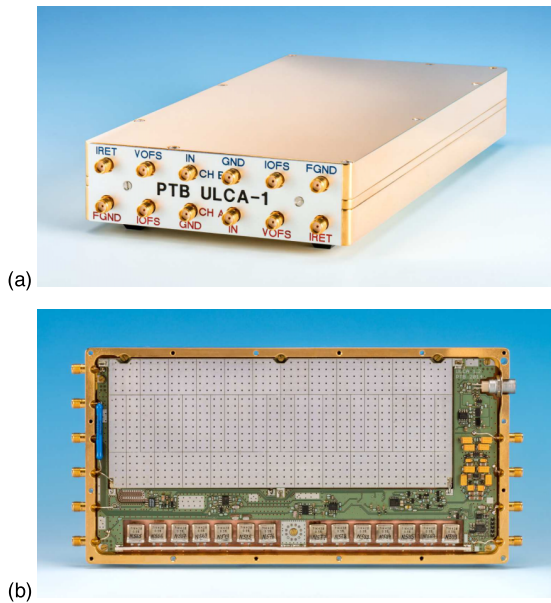


FIG. 2. Photographs of a ULCA prototype. (a) Complete two-channel unit with a total size of $23 \text{ cm} \times 12 \text{ cm} \times 4 \text{ cm}$ (without connectors) and a mass of about $3\frac{1}{2} \text{ kg}$. The housing is milled from solid copper bars to maximize thermal stability. All connections to inputs and outputs of the instrument are made with SMA connectors. (b) Single ULCA channel without cover plate. The resistor network for the 1000-fold current amplification is located under the guard board at top. The metal-foil resistor array for the current-to-voltage conversion is visible at the bottom.

parallel at the low-ohmic side. A total of 48 base elements are connected in series in a meander-like arrangement, yielding total resistances of $3 \text{ G}\Omega$ and $3 \text{ M}\Omega$ for the two sides of the network, respectively. To increase the resistance ratio from $31 \times 32 = 992$ to 1000, a total of 24 resistor pairs (each connected in parallel) are added on the high-ohmic side. Two adjacent base elements share one resistor pair in order to obtain a regular distribution. A high flexibility is attained because the resistor grade, value, or manufacturer can easily be substituted as long as the case size is not changed. For example, the $3 \text{ G}\Omega$ networks involve $2 \text{ M}\Omega$ resistors with $\pm 0.1\%$ tolerance and $\pm 25 \text{ ppm/K}$ temperature coefficient. Lowering the resistance to $200 \text{ k}\Omega$ and keeping the 0805 size, $\pm 0.01\%$ tolerance and $\pm 10 \text{ ppm/K}$ temperature coefficient are available. The resulting $300 \text{ M}\Omega$ networks have improved stability at the expense of an increased noise level (see Sec. IV).

Figure 2 shows photographs of a two-channel ULCA prototype. For maximum thermal stability, the housing is milled from solid copper. The $3 \text{ G}\Omega$ network is covered by top and bottom guard plates. At the bottom of the copper housing in Figure 2(b), the internal $1 \text{ M}\Omega$ standard resistor is visible. It consists of 14 hermetically sealed bulk metal-foil resistors (selected set of VHP101 from Vishay Precision Group). A modular PCB construction was chosen, i.e., both the $3 \text{ G}\Omega$ network and the $1 \text{ M}\Omega$ standard resistor can easily be replaced and tested separately before assembling.

III. BASIC ULCA CONFIGURATIONS

The ULCA was originally intended for the *measurement* of sub-nA currents, only. Recently, it was upgraded with an

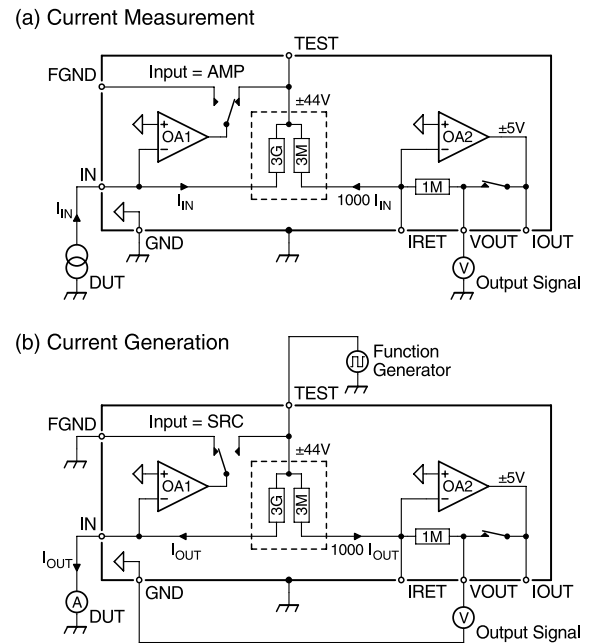


FIG. 3. Basic operation modes of the ULCA with voltage output. (a) Amplifier mode for current measurement, (b) source mode for current generation. In source mode (input = SRC), the IN connector is used for the output current I_{OUT} . Amplifier OA1 forces the voltage at IN to internal ground potential. This ensures that the burden voltage at the DUT does not affect the displayed current measured with a voltmeter between the VOUT and GND connectors.

option for the *generation* of small electric currents. Figure 3 depicts both operation modes, i.e., current measurement (input = AMP) and current generation (input = SRC). For simplicity, the voltage output mode is shown only; current output may be alternatively used according to Figure 1(b). Compared to Figure 1, two connectors were added (TEST and FGND) and a switch was inserted between the output of OA1 and the high-potential side of the $3 \text{ G}\Omega$ network. For current measurement, this switch connects the output of OA1 with the network, i.e., nothing is changed compared to Figure 1. For current output, however, the output of OA1 is connected to external ground (the ULCA's copper housing) and an appropriate voltage from a function generator is applied to the $3 \text{ G}\Omega$ network. This voltage causes an output current I_{OUT} flowing through the high-ohmic side of the $3 \text{ G}\Omega$ network and via the IN connector into the DUT, for example, a picoammeter under calibration. The 1000-fold output current is passed through the $1 \text{ M}\Omega$ feedback resistance of OA2 and a proportional output voltage is measured with a calibrated voltmeter.

Ideally, the DUT acts as a short for the current source. In practice, however, a small burden voltage appears across the DUT due to its finite input resistance. The effect of this burden voltage on the measurement result is eliminated in Figure 3(b) by OA1 providing a virtual ground at the IN connector; the IN connector's potential is thus always equal to the internal reference potential (open triangles). Therefore, the current flowing into the output stage is exactly proportional to the current through the DUT, with a gain equal to the inverse resistance ratio of the $3 \text{ G}\Omega$ network. As the low-potential side of the voltmeter is connected to the internal reference

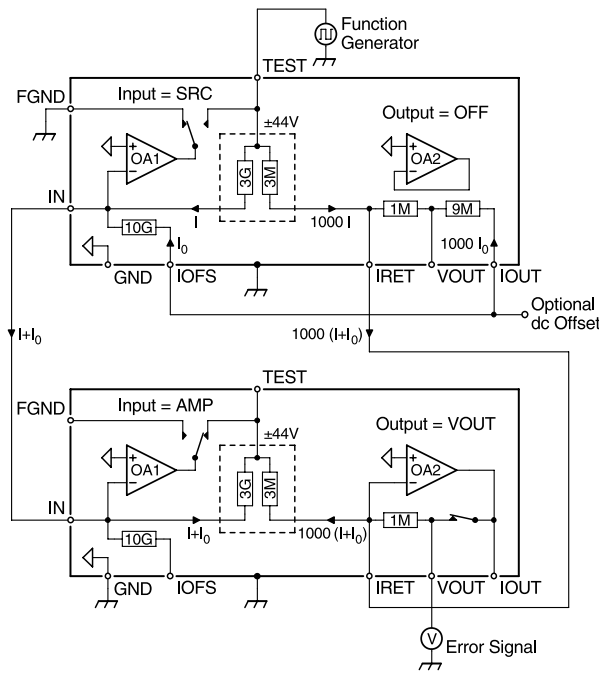


FIG. 4. ULCA self-test configuration for comparing the resistor networks of two ULCA channels with each other. The current-generating ULCA is set into source mode with deactivated output stage (output = OFF). It provides the test currents for the active ULCA set into amplifier mode with voltage output. The output signal (labeled “error signal”) is measured at the VOUT connector. Alternatively, to maximize the output signal, current output with $R_{\text{ext}} = 100 \text{ M}\Omega$ can be used. An optional dc offset may be applied to investigate the linearity of the resistor networks.

potential (and not to the housing), the overall transresistance in SRC mode is identical to that obtained in AMP mode, $A_{\text{TR}} = 1 \text{ G}\Omega$. Note that the amplitude of the output current depends on the burden voltage. This is, however, uncritical because the voltmeter always displays the actual value, i.e., the actual current amplitude multiplied by $A_{\text{TR}} = 1 \text{ G}\Omega$.

A picoammeter can be calibrated with the inherent ULCA accuracy by comparing the currents displayed by the DUT (picoammeter) and the voltmeter. If the DUT and the voltmeter are read out simultaneously, even dynamic effects can be efficiently suppressed, e.g., settling effects after current reversal or low-frequency amplitude fluctuations of the function generator. This relaxes the demands on the function generator considerably. High precision and accurate calibration of the voltmeter are essential, but the function generator does not need calibration. The SRC mode is not only useful for the calibration of picoammeters, but has also practical relevance for consistency tests of the ULCA function: In a two-channel ULCA, one channel may be set into SRC mode to generate a test current for the other channel set into AMP mode. Interchanging the channels then allows mutual consistency tests. Furthermore, a ULCA with a more stable $300 \text{ M}\Omega$ network may be used to calibrate a less accurate $3 \text{ G}\Omega$ unit.

In the SRC mode described above, the accuracy of the voltmeter reading directly enters the overall measurement uncertainty. For the investigation of the input current gain G_I , the most crucial component in the ULCA concept, the demands on the voltmeter performance can be substantially reduced by using a special self-test configuration depicted

in Figure 4. One ULCA is set into SRC mode to generate the input current for the other ULCA (cable between IN connectors). In addition, the 1000-fold amplified input current is passed from the current-generating device into the current-measuring unit (cable between IRET connectors). Ideally, the currents cancel each other at the output stage resulting in zero output. In practice, a small imbalance occurs and the voltmeter displays a weak “error signal” from which the difference in the relative current gain deviations of the two resistor networks can be determined.

The described self-test is intended for *in situ* characterization of resistor networks at highest accuracy but with modest test equipment. The output amplifier OA2 of the current-generating ULCA has to be disconnected from the low-ohmic side of the resistor network, which can be done electronically by setting the output selector into OFF position. Optional offset currents I_0 and $1000 I_0$ can be applied via a voltage at the connectors IOFS and IOU of the current-generating ULCA in Figure 4 (an extra $9 \text{ M}\Omega$ resistor is connected between the VOUT and IOU connectors when the output stage is deactivated). This way, the current amplitudes through the two networks can be made unequal to investigate the current dependence of the relative current gain, i.e., the linearity of the resistor networks at low input currents.

Figure 5 shows a more detailed schematic of the ULCA with all features included. In addition to the optional input offset current (via the $10 \text{ G}\Omega$ thick-film resistor at connector IOFS), an offset voltage may be applied via the VOFS connector. This way, a bias voltage can be applied to the

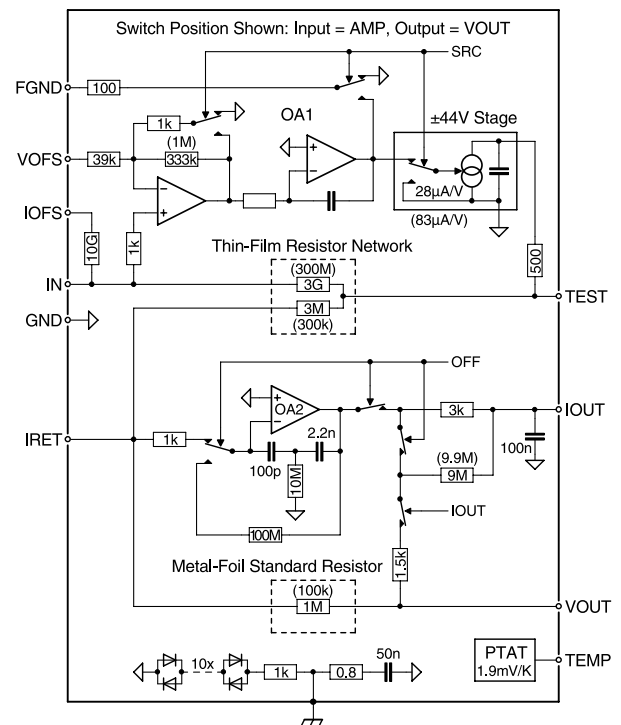


FIG. 5. More detailed schematic of the ULCA. At dc, the internal ground (open triangles) is isolated against the housing so that the reference potential can be defined via the GND input. Resistor values are shown for the low-noise ULCA variant (values in parentheses for the high-accuracy variant). To minimize interference, the circuit is battery powered. All resistances are quoted in ohms and capacitances in farads.

DUT, e.g., to monitor the current-voltage characteristic of an SET device during cool-down. To suppress high-frequency interference, a R - C circuit (0.8Ω and 50 nF) is connected between internal ground and housing. A series connection of ten anti-parallel low-leakage diodes limits the voltage between internal ground and housing to a safe level when the GND connector is left open. All input/output terminals are overvoltage-protected by appropriate series resistors. For the temperature monitoring, the internal voltage reference (AD780 from Analog Devices) is applied that has an analog temperature output proportional to absolute temperature (PTAT). It is buffered and filtered, and made accessible to the user at the TEMP connector. The typical transfer coefficient is 1.9 mV/K ; the actual value is determined during the ULCA's calibration.

Besides the traceable measurement or generation of sub-nA currents, the ULCA also allows the calibration of high-ohmic resistors with ultimate performance. The circuit in Figure 6(a) utilizes the ULCA's internal $1 \text{ M}\Omega$ resistor to compare the resistor under calibration (DUT) against the ULCA's transresistance A_{TR} . At the output, the difference between both appears as the "error signal," i.e., the demands on the voltmeter accuracy are quite modest as the transresistance is chosen to nominally match the resistance of the DUT. The standard $3 \text{ G}\Omega$ ULCA is well suited for direct calibration of $1 \text{ G}\Omega$ resistors. The $300 \text{ M}\Omega$ ULCA is equipped with an internal $100 \text{ k}\Omega$ resistor instead of the standard $1 \text{ M}\Omega$, which allows the calibration of $100 \text{ M}\Omega$ resistors at highest accuracy. If a

sufficiently stable $100 \text{ M}\Omega$ standard resistor is available, the resistance calibration via the ULCA can be verified by a direct calibration with a CCC against the quantum Hall resistance (QHR).⁸ Such a consistency check might help to validate the CCC/ULCA setups or to find previously unknown effects contributing to the measurement uncertainty (e.g., higher leakage currents or stronger settling effects than expected).

For other values of the DUT, an external reference resistor can be used according to Figure 6(b). Here, the DUT is compared against the external standard resistor in a setup similar to the self-test configuration shown in Figure 4. The current-generating ULCA in Figure 4 is replaced by the combination of DUT plus reference resistor that should have a nominal 1000:1 resistance ratio. The output is proportional to the resistance deviation, which reduces the demands on the voltmeter accuracy substantially. For low-ohmic reference resistors, lead resistances have to be considered as discussed in Sec. II for low values of R_{ext} . Before mounting a resistor network into an ULCA, it can be tested with this setup which is convenient for components inspection. If the gain of the ULCA in Figure 6(b) is sufficiently well known, the network under test can be calibrated this way. On the other hand, if a calibrated network (e.g., a more stable $300 \text{ M}\Omega$ network) is available for current generation, the ULCA's current gain can be calibrated without a CCC.

IV. EXPERIMENTAL PERFORMANCE

The ULCA's noise performance was investigated in the frequency range between 1 mHz and 10 Hz , both for the standard $3 \text{ G}\Omega$ resistor network and the $300 \text{ M}\Omega$ high-accuracy variant (Figure 7). The amplifier input was open-circuited and covered by a connector cap to minimize power-line interference. The spectra were measured with a signal analyzer (35665A from Agilent) and the individual time traces were read out and stored for later analysis. Low white noise levels of $2.4 \text{ fA}/\sqrt{\text{Hz}}$ and $7.5 \text{ fA}/\sqrt{\text{Hz}}$ are achieved for the two variants, dominated by Nyquist noise in the resistor networks with a small contribution of $<0.5 \text{ fA}/\sqrt{\text{Hz}}$ from the input amplifier. Note that for a DUT representing a floating current source, each terminal of the source may be connected to a

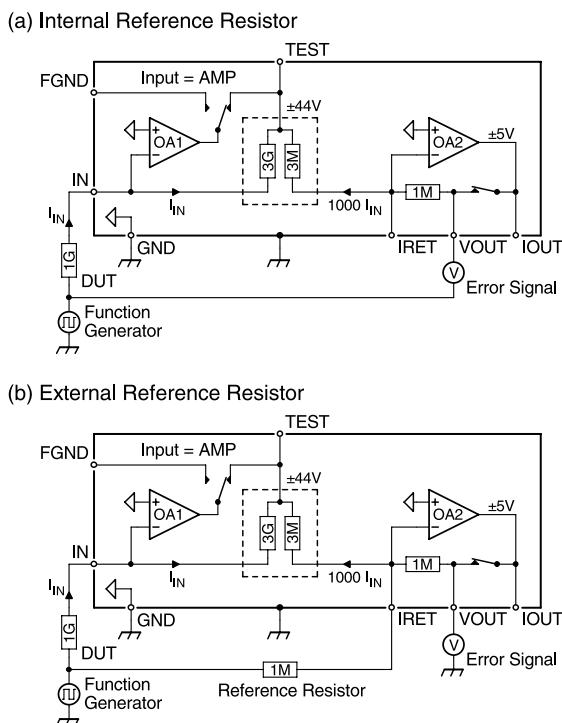


FIG. 6. Calibration of high-ohmic resistors with the ULCA. (a) Internal reference resistor, (b) external reference resistor. In (a), the voltmeter measures the deviation between the resistance of the DUT and the transresistance A_{TR} of the ULCA. The voltage across the DUT is limited by the ULCA output stage to $\pm 5 \text{ V}$. In (b), the DUT is compared against the external reference resistor with a nominal 1000:1 resistance ratio. Here, the voltage across the DUT is limited by the $\pm 44 \text{ V}$ dynamic range of the ULCA input stage.

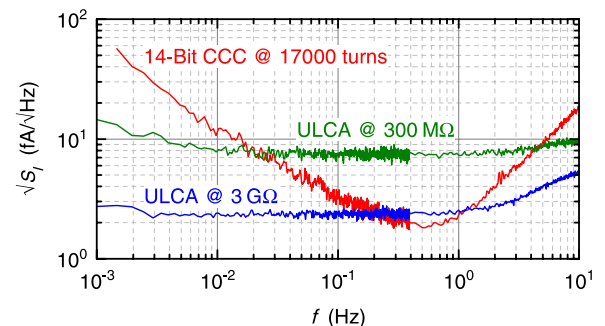


FIG. 7. Input current noise spectra of two ULCA variants ($3 \text{ G}\Omega$ and $300 \text{ M}\Omega$) in comparison with the noise of the PTB 14-bit CCC.⁸ The noise was measured with an HP35665A signal analyzer. For the ULCA, current output with $R_{\text{ext}} = 100 \text{ M}\Omega$ was used to maximize the output signal. For the CCC, an input coil with 17 000 turns was assumed. The CCC noise was measured in a ratio-error test configuration.⁹

separate input of a two-channel ULCA, thus measuring the current twice and increasing the signal-to-noise ratio by a factor of $\sqrt{2}$.¹¹ Furthermore, correlation analysis between the two channels may provide extra information on noise sources in the setup.

At low frequencies, excess noise is commonly observed with a typical frequency dependence of the power spectral density $S \propto 1/f$. The $1/f$ corner is defined as the frequency at which the spectral densities of white noise and low-frequency excess noise are equal, corresponding to a factor of $\sqrt{2}$ increase in overall rms noise. The 3 G Ω ULCA exhibits no noticeable $1/f$ noise component down to about 1 mHz. Its low-frequency noise performance is substantially better than that of the 14-bit CCC wired as a current amplifier with 17 000 input coil turns (cf. Figure 7). The 300 M Ω variant shows $1/f$ noise with a corner frequency of about 2.5 mHz, still better than the 14-bit CCC at frequencies below about 20 mHz. The increased low-frequency noise of the 300 M Ω ULCA is presumably caused by the input amplifier's voltage noise that appears as an extra current noise equal to the noise voltage divided by the network resistance. The low-frequency voltage noise could be suppressed by applying a chopper amplifier at the expense of additional switching noise (i.e., additional current noise).¹²

The Allan deviation is widely used for analyzing noise in low-level measurements. For white noise, it is equal to the standard deviation of the mean σ_w .¹³ It is related to the white noise spectral density S_w by

$$\sigma_w = \sqrt{S_w/2\tau}, \quad (1)$$

where τ is the sampling time. Figure 8 shows Allan deviations calculated from the time traces that were used for the noise spectra in Figure 7. The straight lines in Figure 8 are calculated with Eq. (1) by using the white noise levels determined from the spectra in Figure 7. Excellent agreement between the Allan deviations and the straight lines is obtained at low sampling times τ where the noise is white. The 3 G Ω ULCA exhibits a minimum in the Allan deviation of about 0.1 fA at a sampling time near 1000 s, consistent with an onset of low-frequency excess noise around 1 mHz. Note that the measurements were performed without temperature stabilization. The excellent low-frequency noise is made possible by the solid copper housing of the ULCA combined with a small and stable input

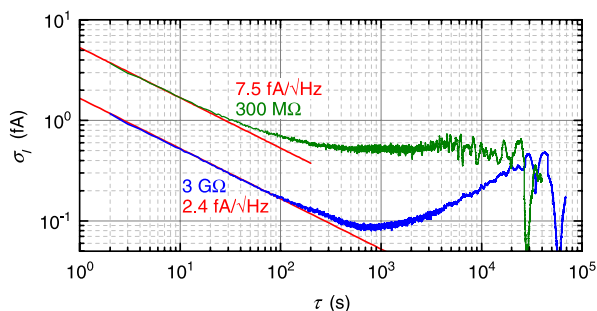


FIG. 8. Allan deviation of the input current noise of the two ULCA's from Figure 7. White noise is indicated by straight lines. The corresponding spectral densities are taken from the noise spectra in Figure 7.

bias current, that has a level of about 20 fA and a temperature coefficient of about 1 fA/K, respectively. For the 300 M Ω ULCA, the Allan deviation levels off at about 0.5 fA for sampling times above a few 100 s caused by $1/f$ amplifier noise.¹³

Generally, for precision dc measurements, the signal to be measured is periodically reversed in order to suppress offset and drift effects. The amplitude of the resulting low-frequency square wave yields the desired dc level. In this paper, raw data analysis according to the method sketched in Figure 7 of Ref. 14 is used to determine the result of dc current measurements with the ULCA. To suppress settling effects after current reversal, a certain number of data points are disregarded after each polarity change. Due to low-frequency excess noise, it is not desirable to make the repetition frequency f_R unnecessarily low. Therefore, excellent settling after polarity reversal is crucial to obtain 0.1 ppm accuracy even with a relatively high repetition frequency $f_R = 0.05$ Hz (typically chosen at PTB for calibrations with the CCC).

The ULCA's resistor network was carefully optimized for minimum settling effects. By appropriate PCB layout, the secondary side of the network is used as a guard for the primary side. As much material as possible is milled away from the resistor board to minimize leakage and dielectric absorption effects. Careful mechanical design results in a still rigid construction. Guard rails on the edges of the resistor board eliminate leakage to the housing at the points of mechanical mounting. Special guard plates made from PCB are placed on top and bottom of the network board. The combination of all these measures yields a stable current gain and an excellent settling behavior for the 3 G Ω resistor network (see Figure 9). Note that the 300 M Ω variant should have a ten times lower dynamic deviation because of its ten times lower resistance as compared to the 3 G Ω network

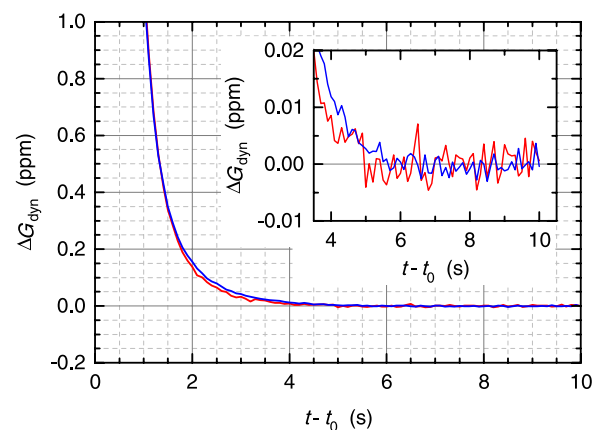


FIG. 9. Settling behavior of a two-channel 3 G Ω ULCA measured with the 14-bit CCC. ΔG_{dyn} is the relative deviation of G_I from its final value after decaying of transients, and $t - t_0$ is the time after current reversal. A square-wave current of ± 13 nA was applied to the ULCA input. About 25 000 or 110 000 individual step responses were averaged for the two channels, respectively. The responses to positive current steps were directly used for averaging, whereas those for negative steps were inverted before taking them into account. The displayed noise bandwidth is 3 Hz (set by a third-order Bessel-type low-pass filter in the nanovoltmeter of the CCC electronics). The inset shows a zoom of the final settling.

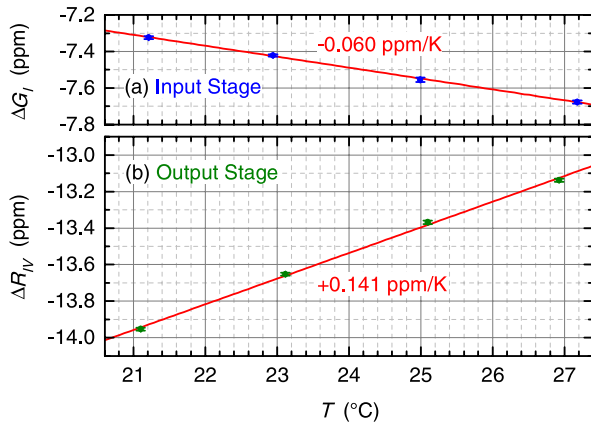


FIG. 10. Temperature dependence of the ULCA transfer coefficients measured with the 14-bit CCC. (a) Relative current gain deviation ΔG_I of the input stage, (b) relative transresistance deviation ΔR_{IV} of the output stage. The ULCA was placed in a temperature-stabilized air bath, and the TEMP output was used to determine the actual circuit temperature. About 1½ h minimum waiting time were inserted after each change of the air bath's set temperature. Error bars indicate type A standard uncertainties.

(assuming equal capacitance and dielectric absorption for both types).

The temperature dependence of the ULCA's transfer coefficients (input gain G_I and output transresistance R_{IV}) is determined during the initial CCC calibration. Figure 10 shows an example for a typical 3 G Ω ULCA. The amplifier was placed in a stabilized air bath, and the temperature was varied between 21 °C and 27 °C at intervals of about 2 °C. Linear fits to the four data points (straight lines in Figure 10) yield the respective temperature coefficients. For the seven 3 G Ω networks fabricated so far, very low temperature coefficients between +0.01 ppm/K and -0.15 ppm/K were found, with an average value of -0.06 ppm/K. The first three 1 M Ω metal-foil resistor arrays of the output stage (all from the same purchase order) showed a negative temperature coefficient close to -0.14 ppm/K. In contrast, two samples from a second purchase order showed a positive coefficient, +0.093 ppm/K and +0.141 ppm/K, respectively. The average of the absolute values of all five samples was 0.13 ppm/K. The low temperature dependence of the transfer coefficients allows accurate measurements even without extra temperature stabilization; the temperature stability of a laboratory air conditioner might be sufficient in most cases. For highest demands, the ULCA's built-in temperature sensor can be used to correct for temperature effects.

V. CALIBRATION WITH A CCC

A special feature of the ULCA is that its transresistance can be directly calibrated with a CCC providing traceability to national standards. At PTB, the calibration is performed with a state-of-the-art CCC resistance bridge developed in collaboration between PTB and the company Magnicon.^{15,16} The suitability of this special setup has been experimentally proven, but other CCC resistance bridges may be alternatively used if the required turns ratios are available. The input and output stages of the ULCA are calibrated separately

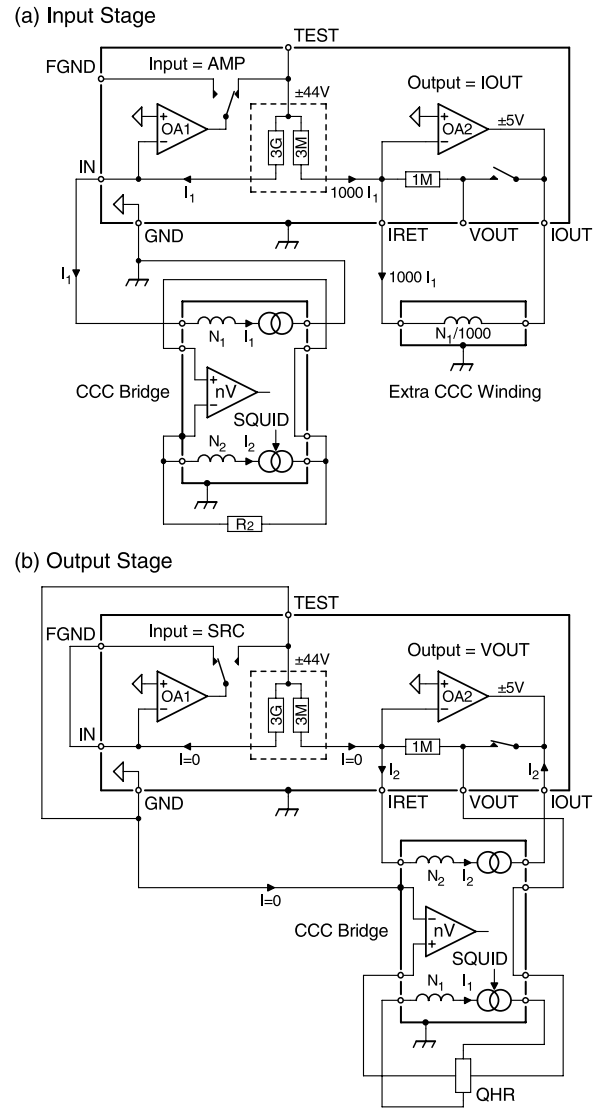


FIG. 11. Calibration of the ULCA with a CCC. (a) G_I of input stage, (b) R_{IV} of output stage. The CCC resistance bridge involves two current sources I_1 and I_2 . A vertical arrow indicates which current source is controlled by the external feedback loop of the SQUID. The negative input of the nanovoltmeter is connected to chassis (solid circle). In (a), an extra CCC winding with a matched number of turns is used to cancel the flux produced by the current I_1 . The resistance bridge measures the gain deviation via the voltage drop across a calibrated resistor R_2 . In (b), R_{IV} is directly compared against the QHR or, optionally, a calibrated standard resistor. The connection between FGND and IN provides feedback for OA1 ensuring adequate operating conditions.

with different setups depicted in Figures 11(a) and 11(b), respectively. The CCC resistance bridge basically consists of two highly isolated current sources (I_1 and I_2) and a low-noise bridge-voltage detector (amplifier labeled “nV”). The currents I_1 and I_2 flow through the respective CCC windings N_1 and N_2 that are coupled to a SQUID. A so-called external feedback loop is realized that keeps the flux in the SQUID constant by controlling one of the current sources.¹⁵ The constant dc flux offset is suppressed by applying current reversal. This way, the current ratio is made exactly equal to the inverse turns ratio, $I_1/I_2 = N_2/N_1$. To enable arbitrary current ratios, a binary compensation network is added that drives an auxiliary winding (not shown in Figure 11 for clarity).¹⁴

The transfer coefficient of the input stage (i.e., the current gain $G_I = 1000$) is a dimensionless quantity. Therefore, it is calibrated by using a pair of CCC windings with a 1000:1 turns ratio, i.e., $N_1 = 4000$ for the 12-bit CCC¹⁵ or $N_1 = 16\,000$ for the 14-bit CCC,⁸ respectively. The current I_1 is passed into GND flowing back through the ULCA input and the N_1 winding; the resulting 1000-fold current at the ULCA's output stage is fed through a winding $N_1/1000$ labeled in Figure 11(a) as “extra CCC winding” because it is not required in case of normal resistance comparisons. The external feedback loop controls current source I_2 . The feedback current is proportional to the deviation of the current gain G_I from the nominal value of 1000. It flows through a standard resistor R_2 , and the resulting voltage drop is measured with the bridge voltage detector. The demands on the accuracy of the standard resistor R_2 are quite modest because the error signal is kept low by the binary compensation unit.¹⁴

The configuration for the calibration of the transfer coefficient of the output stage, $R_{IV} = 1\text{ M}\Omega$, is depicted in Figure 11(b). It resembles a conventional resistance comparison between a $1\text{ M}\Omega$ standard resistor and the QHR, except that the $1\text{ M}\Omega$ resistor is replaced by the ULCA output stage that appears as a virtual $1\text{ M}\Omega$ resistor in a special four-terminal configuration. The current I_2 is passed into the ULCA output stage (IOUT, IRET) and the resulting voltage is tapped between the VOUT and GND connectors. The binary compensation network is adjusted such that the bridge signal is minimized. The residual bridge signal is measured with the bridge voltage detector to determine the resistance ratio. This way, R_{IV} is traced back to the QHR. If a QHR is not available, a calibrated standard resistor may be used instead.

For the ULCA calibration, the currents through the CCC turns are periodically reversed, and the peak-peak amplitude of the resulting output signal is measured. Assuming 50% duty cycle, this means that the sampling time for each of the two current levels is half the total sampling time. In case of white noise, this leads to a factor of $\sqrt{2}$ rise in standard deviation compared to Eq. (1). The standard deviation of the difference between the current levels increases by another factor of $\sqrt{2}$ because the variances of the two current levels are summed up. Therefore, the white noise uncertainty with polarity reversal σ_{PR} is equal to $2\sigma_w$. Generalized one obtains

$$\sigma_{PR} = \sqrt{2S_e/\tau_e}. \quad (2)$$

Here, S_e is the effective white noise density with polarity reversal and τ_e is the effective sampling time without the intervals during which measurement data are disregarded to suppress settling effects after polarity reversal. S_e and S_w are equal for operation in the amplifier's white noise regime, i.e., if the repetition frequency f_R is well above the $1/f$ corner of the amplifier noise. In general, $S_e \approx S(f_R)$ is found; an example is given in Ref. 9 for the 14-bit CCC. To obtain the relative uncertainty, σ_{PR} has to be divided by the peak-peak value of the signal. Note that the relative uncertainty is doubled if the current is switched on and off instead of being reversed because of the halved peak-peak value. For white amplifier noise and negligible settling effects (no disregarded data points after current reversal), equal uncertainties are obtained

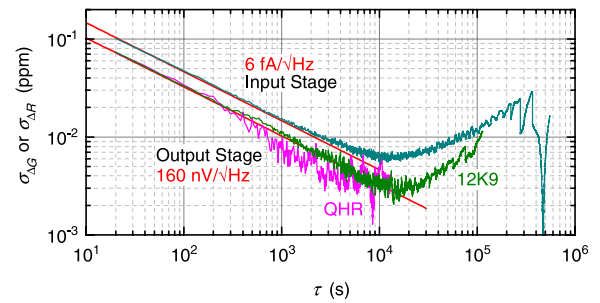


FIG. 12. Allan deviations $\sigma_{\Delta G}$ (input stage) and $\sigma_{\Delta R}$ (output stage) of the relative deviations of the ULCA transfer coefficients measured with the 14-bit CCC. The output stage was calibrated either directly against the QHR or against a $12.9\text{ k}\Omega$ wire-wound standard resistor (curves labeled “QHR” and “12K9”). The current was reversed every 10 s, and the first 5 s after each reversal were disregarded to reject transients. The $3\text{ G}\Omega$ input stage was calibrated at $\pm 13\text{ nA}$, and the $1\text{ M}\Omega$ output stage at $\pm 0.5\text{ V}$ (limited by the allowed current through the QHR). For short measurement times τ , white noise is observed (straight lines). The white noise levels are dominated by CCC current noise (input stage) or Nyquist noise in the $1\text{ M}\Omega$ resistor plus amplifier noise (output stage), respectively.

in a given overall measurement time with and without polarity reversal.

Equation (2) is routinely used to check measurements with polarity reversal for excess noise. Figure 12 depicts Allan deviations obtained from the calibration of ULCA input and output stages. The corresponding white noise levels are $6\text{ fA}/\sqrt{\text{Hz}}$ and $160\text{ nV}/\sqrt{\text{Hz}}$, respectively, in good agreement with the values expected from CCC current noise, Nyquist noise in the $1\text{ M}\Omega$ feedback resistor, plus voltage and current noise from the ULCA's operational amplifiers. All CCC calibrations presented in this section were performed with the PTB 14-bit CCC; alternatively, a 12-bit CCC may be used at the expense of a 4-fold rms current noise and a 4-fold uncertainty contribution from noise rectification in the SQUID.⁹ The ULCA to be calibrated was always placed in a temperature-stabilized air bath, typically at $23\text{ }^\circ\text{C}$.

To illustrate the ULCA's long-term stability, the raw data of a series of input stage calibrations performed over a period of 55 days are depicted in Figure 13 together with a smoothed curve. A drift of -1 ppm/yr is extrapolated from the 55 days period. During the initial calibration (about two

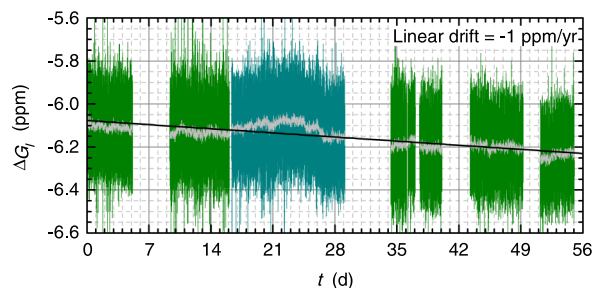


FIG. 13. Stability of the relative current gain deviation ΔG_I of the input stage measured with the 14-bit CCC. Raw data over a period of 55 days are shown together with a moving average over 101 data points ($\tau = 2020\text{ s}$) and a straight line fit indicating the extrapolated long-term drift. In the gaps between the calibration runs, the CCC system was used for other tasks. The longest uninterrupted measurement (days 16 to 29) was used for calculating the Allan deviation $\sigma_{\Delta G}$ in Figure 12.

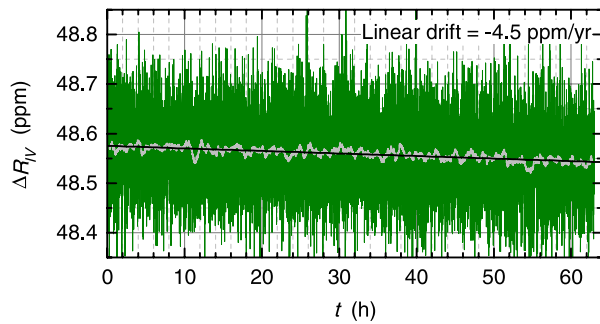


FIG. 14. Stability of the relative transresistance deviation ΔR_{IV} of the output stage during a long CCC calibration. The raw data used for the curve labeled “12K9” in Figure 12 are shown together with a moving average over 101 data points ($\tau = 2020$ s) and a straight line fit indicating the extrapolated long-term drift.

months prior to $t = 0$ in Figure 13), the relative gain deviation of the particular 3 G Ω network chosen for the tested ULCA was about -5.9 ppm. For all seven 3 G Ω networks fabricated so far, relative current gain deviations between -25.3 ppm and $+0.2$ ppm were found during initial calibration, with a typical (average) value of about -9 ppm. The slightly negative average gain deviation could be caused a small contribution from leakage resistance at the high-ohmic sides of the networks. So far we did not notice a correlation between the absolute levels of gain deviation, long-term stability, and temperature dependence of a network.

For the output stage, a similarly long calibration measurement was not possible due to the high degree of utilization of the CCC resistance bridge. The raw data of the longest available output stage calibration (curve labeled “12K9” in Figure 12) are displayed in Figure 14. A clear drift is observable, even within the relatively small period of 63 h. Surprisingly, the extrapolated drift of -4.5 ppm/yr for this short period is in fair agreement with the drift determined from the first half year of operation (between -3 ppm/yr and -4 ppm/yr for the first three prototypes equipped with metal-foil resistors from the same purchase order). Note that the 12.9 k Ω wire-wound standard resistor used for the calibration exhibits a negligibly small drift of about $+0.015$ ppm/yr (measured over a period of twenty years).

VI. CONCLUSIONS

The ULCA is a powerful and flexible tool for the measurement or generation of small electric currents. It can be calibrated with a CCC and features excellent stability of its transresistance A_{TR} . The ULCA provides a hitherto unrivalled accuracy, even when compared to the best sub-nA current measurements reported so far.³ The accuracy of commercial instruments is outperformed by about two orders of magnitude.¹ Compared to current amplification with a CCC alone, the ULCA offers better noise performance at low frequencies and overcomes the limitation set by the systematic uncertainty contribution in a CCC setup at very low currents due to noise rectification in the SQUID.⁹

The ULCA, when configured for current sourcing, may be an attractive alternative to the capacitor charging

method commonly used by NMIs for calibrations in the sub-nA regime.² Here, the ULCA concept avoids the limiting uncertainty contribution from the frequency dependence of the capacitance.⁹ Furthermore, it allows the generation of arbitrary wave forms. Another potential ULCA application is the calibration of high-ohmic resistors. In this application, even if the ULCA is calibrated with a conventional CCC bridge¹⁵ only, a performance is expected that is comparable to CCC bridges specially designed for high-ohmic resistors of up to 1 G Ω .^{17,18}

The superior ULCA performance not only offers benefits for calibration applications but also has implications for fundamental metrology research. For the development of SET devices, it becomes increasingly important to accurately measure their current-voltage characteristics in order to predict the achievable uncertainty on the basis of theoretical models (see, for example, Ref. 19). The handy ULCA is well suited for such measurements, allowing ppm resolution at 100 pA with acceptable averaging times. Finally, the ULCA is also a promising candidate for a direct quantum metrology triangle experiment.²⁰ Within an averaging time of about one day, an uncertainty of 0.1 ppm seems feasible at 100 pA.⁹ Such an accuracy is not achievable with any other instrumentation currently available.

ACKNOWLEDGMENTS

The authors are indebted to Martin Götzt, Monique Klemm, Gerhard Muchow, Eckart Pesel, Michael Piepenhagen, and Bernhard Smandek for their valuable contributions. This work was partially done within Joint Research Project “Qu-Ampere” (SIB07) supported by the European Metrology Research Programme (EMRP). The EMRP is jointly funded by the EMRP participating countries within EURAMET and the European Union.

¹G.-D. Willenberg, “EUROMET.EM-S24: Supplementary comparison of small current sources (report),” *Metrologia* **50**, 01002 (2013).

²G.-D. Willenberg, H. N. Tauscher, and P. Warnecke, “A traceable precision current source for currents between 100 nA and 10 pA,” *IEEE Trans. Instrum. Meas.* **52**, 436–439 (2003).

³S. P. Giblin, M. Kataoka, J. D. Fletcher, P. See, T. J. B. M. Janssen, J. P. Griffiths, G. A. C. Jones, I. Farrer, and D. A. Ritchie, “Towards a quantum representation of the ampere using single electron pumps,” *Nat. Commun.* **3**, 930 (2012).

⁴L. Fricke, M. Wulf, B. Kaestner, F. Hohls, P. Mirovsky, B. Mackrodt, R. Dolata, T. Weimann, K. Pierz, U. Siegner, and H. W. Schumacher, “Self-referenced single-electron quantized current source,” *Phys. Rev. Lett.* **112**, 226803 (2014).

⁵See <http://www.ptb.de/emrp/868.html> for Joint Research Project *Qu-Ampere* (SIB07) conducted within the European Metrology Research Programme (EMRP).

⁶J. Gallop and F. Piquemal, “SQUIDS for standards and metrology,” in *The SQUID Handbook*, edited by J. Clarke and A. I. Braginski (Wiley-VCH, Weinheim, Germany, 2006), Vol. II, pp. 101–114.

⁷F. Renguez, O. Séron, L. Devoille, D. Placko, and F. Piquemal, “A femto ampere current amplifier based on a 30 000:1 cryogenic current comparator,” in *Digest of 29th Conference on Precision Electromagnetic Measurements, Rio de Janeiro, Brazil* (IEEE, 2014), pp. 296–297.

⁸M. Götzt, E. Pesel, and D. Drung, “A compact 14-bit cryogenic current comparator,” in *Digest of 29th Conference on Precision Electromagnetic Measurements, Rio de Janeiro, Brazil* (IEEE, 2014), pp. 684–685.

⁹D. Drung, M. Götzt, E. Pesel, and H. Scherer, “Improving the traceable measurement and generation of small direct currents,” *IEEE Trans. Instrum. Meas.* (submitted).

- ¹⁰D. Drung, “Verstärker zum Verstärken kleiner elektrischer Ströme,” German patent application 10 2012 020 148.6 (17 April 2014), available at <https://register.dpma.de/DPMAregister/pat/PatSchrifteneinsicht?docId=DE102012020148A1>.
- ¹¹D. Drung, C. Krause, U. Becker, H. Scherer, and F. J. Ahlers, “Ultrastable low-noise current amplifier,” in *Digest of 29th Conference on Precision Electromagnetic Measurements, Rio de Janeiro, Brazil* (IEEE, 2014), pp. 656–657.
- ¹²D. Drung and C. Krause, “Excess current noise in amplifiers with switched input,” *IEEE Trans. Instrum. Meas.* (to be published).
- ¹³T. J. Witt, “Using the Allan variance and power spectral density to characterize dc nanovoltmeters,” *IEEE Trans. Instrum. Meas.* **50**, 445–448 (2001).
- ¹⁴D. Drung, M. Götz, E. Pesel, H.-J. Barthelmeß, and C. Hinnrichs, “Aspects of application and calibration of a binary compensation unit for cryogenic current comparator setups,” *IEEE Trans. Instrum. Meas.* **62**, 2820–2827 (2013).
- ¹⁵M. Götz, D. Drung, E. Pesel, H.-J. Barthelmeß, C. Hinnrichs, C. Aßmann, M. Peters, H. Scherer, B. Schumacher, and T. Schurig, “Improved cryogenic current comparator setup with digital current sources,” *IEEE Trans. Instrum. Meas.* **58**, 1176–1182 (2009).
- ¹⁶D. Drung, M. Götz, E. Pesel, J.-H. Storm, C. Aßmann, M. Peters, and Th. Schurig, “Improving the stability of cryogenic current comparator setups,” *Supercond. Sci. Technol.* **22**, 114004 (2009).
- ¹⁷N. E. Fletcher, J. M. Williams, and T. J. B. M. Janssen, “A cryogenic current comparator resistance ratio bridge for the range 10 k Ω to 1 G Ω ,” in *Digest of 22th Conference on Precision Electromagnetic Measurements, Sydney, Australia, May* (IEEE, 2000), pp. 482–483.
- ¹⁸F. L. Hernandez-Marquez, M. E. Bierzychudek, G. R. Jones, Jr., and R. E. Elmquist, “Precision high-value resistance scaling with a two-terminal cryogenic current comparator,” *Rev. Sci. Instrum.* **85**, 044701 (2014).
- ¹⁹V. Kashcheyevs and J. Timoshenko, “Quantum fluctuations and coherence in high-precision single-electron capture,” *Phys. Rev. Lett.* **109**, 216801 (2012).
- ²⁰H. Scherer and B. Camarota, “Quantum metrology triangle experiments: A status review,” *Meas. Sci. Technol.* **23**, 124010 (2012).

Review of Scientific Instruments is copyrighted by AIP Publishing LLC (AIP). Reuse of AIP content is subject to the terms at: <http://scitation.aip.org/termsconditions>. For more information, see <http://publishing.aip.org/authors/rights-and-permissions>.